Kobe University Repository : Kernel

PDF issue: 2025-12-05

A compressible solver for the laminar-turbulent transition in natural convection with high temperature differences using implicit large eddy simulation

Li, Chung-Gang

(Citation)
International Communications in Heat and Mass Transfer,117:104721

(Issue Date)
2020-10

(Resource Type)
journal article

(Version)
Accepted Manuscript

(Rights)
© 2020 Elsevier Ltd.
This manuscript version is made available under the CC-BY-NC-ND 4.0 license
http://creativecommons.org/licenses/by-nc-nd/4.0/

(URL)
https://hdl.handle.net/20.500.14094/90008796

KOBE UNIVERSITY

A Compressible Solver for the Laminar–turbulent Transition in Natural Convection with High Temperature Differences Using Implicit Large Eddy Simulation

Chung-Gang Li

Department of Computational Science, Graduate School of System Informatics, Kobe University, 1-1 Rokkodai, Nada-ku, Kobe 657-8501, Japan

Correspondence to: Chung-Gang Li
Computational Fluid Dynamics Laboratory
Department of Computational Science
Graduate School of System Informatics
Kobe University, 1-1 Rokkodai, Nada-ku,
Kobe 657-8501, Japan
E-mail: cgli@aquamarine.kobe-u.ac.jp
+81-78-803-6680

ABSTRACT

The transition induced by the natural convection with high temperature differences can be easily observed in many engineering applications. The compressible solver has to be taken into consideration because the usual way of using the incompressible solver with Boussinesq approximation is only available within the temperature difference of 30K. However, speeds in natural convection are always several orders of magnitude lower than the speed in compressible regions. A modified compressible solver which can deal with the buoyancy-induced turbulence is proposed here. In this solver, an all speed preconditioned Roe (APRoe) is adopted to appropriately treat flows at extremely low speed regions. And then, a reconstruction method for the MUSCL scheme at low Mach numbers (M5LM) is applied to attenuate the dissipation. The numerical dissipation of the compressible solver is utilized as a subgrid scale (SGS) model for the implicit large eddy simulation (LES). Based on qualitative agreement with direct numerical simulation and considering the capability of numerically predicting a −3 decay law for the energy transfer induced by the natural convection in the temporal power spectrum of the temperature fluctuation, this solver is potentially a good candidate for laminar–turbulent transition in natural convection.

Keywords: laminar-turbulent transition, natural convection, compressible solver, Roe, implicit LES

1. Introduction

The laminar–turbulent transition in natural convection is a critical phenomenon encountered in diverse engineering applications, such as solar energy collection, chimney design, and the thermal analysis of fins. Simulating this transition remains a challenge because of densities vary in regions of very low speed and the transition to turbulence. Concerning engineering applications, the temperature differences responsible for variations in density in natural convection always exceed the limits regarding the validity of the incompressible solver with the Boussinesq approximation (30 K) [1]. A compressible-flow solver that is specific to extremely low Mach numbers is therefore needed as the contribution of buoyancy to flow speeds is always several orders of magnitude smaller than the speed of sound. The other troublesome issue is the transition to turbulence. Flow fields in engineering applications always have three stages: laminar, transition, and turbulent stages. Only a turbulence model that captures these three different stages accurately can be considered.

Because of the complexity of numerical methods and limited computational resources, relatively few studies have been conducted on buoyancy-induced flows with larger temperature differences using compressible-flow solvers. Weiss and Smith [2] applied a preconditioning matrix in the Roe scheme [3] to simulate natural convection with temperature differences of 1000 K. Their results indicate that using a compressible-flow solver in natural convection becomes feasible as the preconditioning method tremendously reduces the computational time. Paillere and co-workers [4] used a preconditioning method originally developed by Turkel [5] to investigate natural convection in enclosures with a high temperature (600 K). They concluded that with lower temperature differences, results obtained using incompressible-flow solvers applying the Boussinesq approximation are almost identical to those obtained using compressible-flow solvers applying the

preconditioning method. The foregoing literature is limited to laminar flow fields of relatively low Rayleigh (or Reynolds) numbers.

Another issue of simulations is how to accurately capture flow fields in the laminar–transition–turbulence passage. Li and co-workers [6] simulated natural convection in a vertical channel; transitional phenomena were successfully captured by conducting compressible direct numerical simulation (DNS). However, DNS is neither appropriate nor efficient from the point of view of engineering applications. Compared with DNS, LES is more adaptable for use in simulating transitional phenomena and time-evolving turbulent flow. Lau and co-workers [7,8] adopted LES to use the same physical model as used in [6] to investigate the reliability of the sub-grid scale (SGS) model for the buoyancy-induced transition. They found that the Vreman model [9] is more suitable than the Smagorinsky model, dynamic model, and approximate localized dynamic model. However, the coefficient for the eddy viscosity in the Vreman model still needs to be determined through trial and error. Pham et al. [10] used LES with SGS models including the Smagorinsky model, the dynamic model, the Lagrangian dynamic model [11], and the extended Lagrangian dynamic model [12] in a turbulent natural convection flow with the Grashof number (Gr) = 2.2×10^{10}. Their results indicate that the extended Lagrangian dynamic model performs better than the other models, especially in the turbulent region. The foregoing LES literature on turbulent flows induced by buoyancy is based on explicit turbulence modelling. Such modelling uses a dissipative mechanism to remove the unphysical energy accumulating at smaller scales [13]. However, the numerical scheme for compressible-flow solvers is generally more dissipative than that for incompressible-flow solvers. Hence, explicit turbulence modelling using compressible solvers without modification usually affects results adversely through the over-dissipation. To resolve the over-dissipation issue, implicit LES offers an

alternative approach. To date though, no study has surfaced adopting the implicit LES for buoyancy-induced turbulent flows.

Therefore, the present study proposes a compressible solver for the laminar-turbulent transition in natural convection using implicit LES based on RoeAP [14] and M5LM [15]. The simulations of the expanding thermal plume are conducted to validate the current numerical method. The results show qualitative agreement with direct numerical simulation results indicating that the current solver is potentially a good candidate for using implicit LES on laminar–turbulent transition in natural convection with high temperature differences.

2. Model and governing equations

A rectanguloid (Fig. 1(a)) has a circular heat source of diameter D situated at the bottom and open boundaries on all other sides. The origin is set at the centre of the heat source. The streamwise and two spanwise directions are labelled x_1, x_2 and x_3 while the flow velocities in these directions are respectively denoted, u_1, u_2 and u_3. Gravity acts in the negative x_1 direction.

The model follows the basic setup described in [10] and [16] within a DNS setting. No-slip and isothermal boundary conditions are applied to the bottom wall. The temperature distribution is assigned adopting the suggestion given in [10]:

$$T = 0.5(T_h - T_0) \times \{1 - \tanh[b_2(2r/D - D/(2r))]\} + T_0, \quad (1)$$

where r is the distance from the centre point, T_h is 673 K, T_0 is the ambient temperature, set at 298.06 K, and b_2 is a constant set at 6.25.

For the other boundary, the absorbing boundary condition for low speeds developed by Li et al. [6] and Fu et al. [17] at the outmost regions of the computational domain is used to prevent reflections contaminating the result. The related parameters used in this study are listed in Table 1.

The governing equations are the original Navier–Stokes equations without any additional terms except for numerical dissipation for modelling the SGS effects:

$$\frac{\partial U}{\partial t} + \frac{\partial F_1}{\partial x_1} + \frac{\partial F_2}{\partial x_2} + \frac{\partial F_3}{\partial x_3} = S. \quad (2)$$

The quantities included in U, F_i, and S are

$$U = \begin{pmatrix} \rho \\ \rho u_1 \\ \rho u_2 \\ \rho u_3 \\ \rho e \end{pmatrix} \quad F_i = \begin{pmatrix} \rho u_i \\ \rho u_i u_1 + p\delta_{i1} - \mu A_{i1} \\ \rho u_i u_2 + p\delta_{i2} - \mu A_{i2} \\ \rho u_i u_3 + p\delta_{i3} - \mu A_{i3} \\ (\rho e + p)u_i - \mu A_{ij} u_j - k\partial T/\partial x_i \end{pmatrix} \quad S = \begin{pmatrix} 0 \\ -(\rho - \rho_0)g \\ 0 \\ 0 \\ -(\rho - \rho_0)g u_1 \end{pmatrix}, \quad (3)$$

where $A_{ij} = \partial u_i / \partial x_j + \partial u_j / \partial x_i - 2/3(\nabla \cdot u)\delta_{ij}$ and p is the pressure given by the ideal gas equation, $p = \rho RT$. The viscosity and thermal conductivity of the fluid are based on Sutherland's law:

$$\mu(T) = \mu_0 (T / T_0)^{3/2} [(T_0 + 110) / (T + 110)], \tag{4}$$

$$k(T) = \mu(T)\gamma R / [(\gamma - 1)Pr], \tag{5}$$

where $\rho_0 = 1.1842 kg/m^3$, $g = 9.81 m/s^2$, $\mu_0 = 1.85 \times 10^{-5} N \cdot s/m^2$, $T_0 = 298.06 K$, $\gamma = 1.4$, $R = 287 J/kg/K$, and $Pr = 0.72$.

3. Numerical method

In low-speed regions of nearly incompressible flows, the fluid speed contributed through buoyancy is several orders of magnitude lower than that in the compressible region. The Roe scheme with a preconditioning method and dual time stepping [2] is applied to resolve Eq. (2). Hence, the new governing equation is

$$\Gamma\frac{\partial U_p}{\partial\tau}+\frac{\partial U}{\partial t}+\frac{\partial F_1}{\partial x_1}+\frac{\partial F_2}{\partial x_2}+\frac{\partial F_3}{\partial x_3}=S; \tag{6}$$

where Γ is the preconditioning matrix proposed by Weiss and Smith [2], U_p the primitive form $[P,u_1,u_2,u_3,T]$, τ and t are the artificial and physical times, respectively, and U the conservative form of $[\rho,\rho u_1,\rho u_2,\rho u_3,\rho e]$.

The discretized form of Eq. (6) is

$$\begin{aligned}&\Gamma\frac{\overline{U}_p^{k+1}-\overline{U}_p^{k}}{\Delta\tau}+\frac{3\overline{U}^{k+1}-4\overline{U}^{n}+\overline{U}^{n-1}}{2\Delta t}+\frac{1}{\Delta x_1}(\overline{F}_{1(i+1/2,j,k)}^{k+1}-\overline{F}_{1(i-1/2,j,k)}^{k+1})\\&+\frac{1}{\Delta x_2}(\overline{F}_{2(i,j+1/2,k)}^{k+1}-\overline{F}_{2(i,j-1/2,k)}^{k+1})+\frac{1}{\Delta x_3}(\overline{F}_{3(i,j,k+1/2)}^{k+1}-\overline{F}_{3(i,j,k-1/2)}^{k+1})=0\end{aligned}. \tag{7}$$

The superscripts k and n indicate the iteration numbers of artificial time and the proceeding step of real time, respectively. When the term $\partial U_p/\partial\tau$ converges to zero, the quantities associated with the artificial time term of the $(k+1)th$ iteration are transferred approximately to quantities of the $(n+1)th$ time step in real time, reducing Eq. (6) to the original Navier–Stokes equation including the transient term.

Finally, Eq. (6) can be rearranged as

$$[\frac{I}{\Delta\tau}+\Gamma^{-1}M\frac{3}{2\Delta t}+\Gamma^{-1}(\delta_{x_1}A_p^k+\delta_{x_2}B_p^k+\delta_{x_3}C_p^k)]\Delta U_p=\Gamma^{-1}R^k; \tag{8}$$

where $M=\partial U/\partial U_p$, δ_{x_i} the central-difference operator, $A_p=\partial F_1^k/\partial U_p$ the flux Jacobian, and $R^k=-(3U^k-4U^n+U^{n-1})/(2\Delta t)-(\delta_{x_1}\overline{F}_1^k+\delta_{x_2}\overline{F}_2^k+\delta_{x_3}\overline{F}_3^k)$. Eq. (8) is

solved using the Lower-Upper Symmetric-Gauss-Seidel (LUSGS) implicit method.

In the calculation of R^k on the right-hand side of Eq. (8), the terms involving F_i in Eq. (3) can be divided into an inviscid term $F_{inviscid}$,

$$F_{inviscid} = \begin{pmatrix} \rho u_i \\ \rho u_i u_1 + p\delta_{i1} \\ \rho u_i u_2 + p\delta_{i2} \\ \rho u_i u_3 + p\delta_{i3} \\ (\rho e + p)u_i \end{pmatrix} \tag{9}$$

and a viscous term $F_{viscous}$,

$$F_{viscous} = -\begin{pmatrix} 0 \\ \mu A_{i1} \\ \mu A_{i2} \\ \mu A_{i3} \\ \mu A_{ij} u_j + \lambda \dfrac{\partial T}{\partial x_i} \end{pmatrix}. \tag{10}$$

The Roe scheme is employed in discretizing $F_{inviscid}$,

$$F_{inviscid,i+1/2} = \frac{1}{2}[F_R(U) + F_L(U)] + F_d, \tag{11}$$

where F_d is the Roe dissipation term, which is composed of jumps of properties of work fluids.

For the reconstruction of F_R and F_L, the fifth-order MUSCL scheme (the monotonic upstream-centred scheme for conservation laws proposed by Kim and Kim [18]) without a limiter function to prevent turbulent fluctuations from attenuating, is adopted and expressed as

$$U_{L,i+1/2} = 1/60 \times (2U_{i-2} - 13U_{i-1} + 47U_i + 27U_{i+1} - 3U_{i+2}), \tag{12}$$

$$U_{R,i-1/2} = 1/60 \times (-3U_{i-2} + 27U_{i-1} + 47U_i - 13U_{i+1} + 2U_{i+2}). \quad (13)$$

However, even without a limiter function, the MUSCL scheme is still too dissipative for the simulation of turbulent flows because of the discontinuous jump between U_R and U_L. The modification using M5LM [15] to improve the phenomenon of the over-dissipation is relocated as detailed in the next section.

Aside from the inviscid term, the derivative terms in A_{ij} in the viscous term of Eq. (3) are calculated using the second-order central difference.

4. Implicit LES using the Roe dissipation term F_d

Following [14], F_d in x_1 direction in Eq. (11) is written as

$$F_{d,x_1} = -\frac{1}{2}\{[|U_{IC}|\begin{bmatrix}\Delta\rho\\ \Delta(\rho u_1)\\ \Delta(\rho u_2)\\ \Delta(\rho u_3)\\ \Delta(\rho E)\end{bmatrix}] + \delta U\begin{bmatrix}\rho\\ \rho u_1\\ \rho u_2\\ \rho u_3\\ \rho H\end{bmatrix} + \delta p\begin{bmatrix}0\\ 1\\ 0\\ 0\\ u_1\end{bmatrix}\}, \tag{14}$$

where U_{IC} is the cell interface velocity determined by the Roe-averaged variables [3] and $\Delta()$ is the discontinuous jump between the right and left states calculated from Eq.(12) and Eq. (13). δU and δp for the APRoe [14], which has been proved to be more accurate for the simulation of the natural convection than that of the original preconditioning Roe scheme in [19], are as below.

$$\delta U = (\tilde{c} - \frac{1-\theta}{2}u_1\frac{\tilde{U}}{\tilde{c}} - \theta|u_1|)\frac{\Delta p}{\rho\theta c^2} + \frac{U'}{\tilde{c}}\Delta u_1, \tag{15}$$

$$\delta p = \frac{U'}{\tilde{c}}\Delta p + (c' - |u_1| + \frac{1-\theta'}{2}u_1\frac{U'}{\tilde{c}})\rho\Delta u_1, \tag{16}$$

where $\theta = \min[\max(M_{ref}{}^2, M^2), 1]$, $\theta' = \min[M^2, 1]$, M is the local Mach number and M_{ref} is a global Mach parameter, which can be calculated according to the characteristic velocity, $U_0 = \sqrt{gD\Delta T / T_0}$. Δu_1 and Δp are the discontinuous jump of the velocity $(u_{1,R} - u_{1,L})$ and the pressure $(p_R - p_L)$. Additionally, c the speed of sound, $c' = 1/2\sqrt{4c^2\theta' + (1-\theta')^2 u_1{}^2}$, $\tilde{c} = \min[\max(M_{ref}{}^2, M^2), 1]c$ and $U' = 1/2(1+\theta')u_1$.

In terms of numerical simulation, because both of the Roe dissipation term and the SGS model do the same thing which is to provide the dissipation, the Roe dissipation term has the capability of removing the redundant energy at the smaller scale if the magnitude of F_d is appropriately controlled [20,21]. However, the

compressible solver always provides too much dissipation at extremely low speed regions such as natural convection problems even with the modification of the preconditioning method.

To solve the over-dissipation issue, M5LM proposed by Thornber et al. [15] is applied to the reconstruction. When examining Eq. (14), (15) and (16), it can be known that the dissipation can be reduced by decreasing the discontinuous jump of Δu_1 and Δp. M5LM modifies the reconstructed velocity in Eq. (12) and (13) to decrease the discontinuous jump as the following.

$$u_{1,L,\mathrm{M5LM}} = \frac{u_{1,L} + u_{1,R}}{2} + \mathrm{z}\frac{u_{1,L} - u_{1,R}}{2}, \tag{17}$$

$$u_{1,R,\mathrm{M5LM}} = \frac{u_{1,L} + u_{1,R}}{2} + \mathrm{z}\frac{u_{1,R} - u_{1,L}}{2}. \tag{18}$$

Where z is the local Mach number at the cell interface. With this modification, the discontinuous jump between $u_{1,L}$ and $u_{1,R}$ can be reduced and the Roe dissipation term of the APRoe can be greatly improved to be an implicit turbulence model.

5. Results and discussion

Three different solvers, including two implicit LES models and one explicit model, are tested to evaluate their performance. For the implicit LES models, APRoe with M5LM is forthwith referred to as M5LM-APRoe and APRoe without M5LM is referred to as M5-APRoe. For the explicit model, M5LM-APRoe with a classical Smagrinsky model as the SGS model is referred to as M5LM-APRoe-SGS. For the Smagorinsky constant C_S, a classical value is 0.2. However, larger dissipation is generated by this value and a lower value 0.11 is suggested by Canuto and Cheng [22]. Besides, Bui [23] and Fu et al. [24] also adopted C_S=0.1 for the compressible solver to obtain accurate results. Therefore, C_S=0.1 is finally adopted in the present study. The results of DNS obtained by Pham and co-workers [10] are compared with the results of the present simulation. The grid number adopted in [10] are also listed in Table 1.

Figure 1(a) shows the vorticity iso-surface contoured using the velocity magnitude of the M5LM-APRoe simulation. The transition occurs after $x_1>D$ and the hairpin-shaped structures mainly form in the vortex regions when $x_1>4D$. This observation is basically consistent with that in [10]. Overall, the buoyancy-induced evolution from laminar to turbulence can be clearly observed using the M5LM-APRoe.

Figure 1(b) compares the development of the vorticity isosurface contoured using the velocity magnitude among M5LM-APRoe, M5LM-APRoe-SGS and M5-APRoe. In the laminar region of x_1 < 2D, for the M5LM-APRoe and M5LM-APRoe-SGS, the unsteady concentration of vorticity develops and gradually enlarges up to x_1 = 2D, which is consistent with the description in [10]. Meanwhile, for M5-APRoe, the unsteady phenomenon only occurs around x_1 = 2D. Additionally, according to DNS results [10], the transition from laminar flow to turbulence is

located close to x_1 = 3D. This phenomenon is most obvious for M5LM-APRoe. In the turbulence region of x_1 > 4D, hairpin vertical structures dominate the flow field and interlace with each other [10] and M5LM-APRoe and M5LM-APRoe-SGS capture this phenomenon more completely than does M5-APRoe. However, for M5LM-APRoe-SGS, because extra dissipation is added by the SGS model, comparing with the M5LM-APRoe, the smaller turbulent structures are wiped out.

Fig. 2 compares the present results with the DNS results [10] in terms of the normalized profiles of mean temperature and mean velocity u_1 along the plume centreline axis. The mean temperature is normalized using (T-T_0)/ (T_h-T_0), and the mean velocity is normalized using the characteristic buoyant velocity, $U_0 = \sqrt{gD\Delta T / T_0}$. For the mean temperature profile, the M5LM-APRoe and M5LM-APRoe-SGS produce distribution in better agreement with the DNS result than does M5-APRoe. However, because the classical Smagorinsky model is not so suitable near the wall especially without a damping term, the negative effect close to the wall ($x_1 / D = 0$) is observed. Hence, according to the distribution of the mean temperature, M5LM without the SGS model can capture the most accurate result. For the mean velocity profile, the same conclusion can be made that M5LM-APRoe can have the best result among these three solvers.

The curves of turbulence intensity versus temperature and velocity along the plume centreline axis (Fig. 3) show that the M5LM-APRoe mitigates the overestimation of M5-APRoe. This is because in the thermal plume, the flow filed is anisotropic and the over-dissipation of M5-APRoe enlarges the turbulent structure shown in Fig. 1(b) such that the turbulent fluctuations in the streamwise direction are overestimated. Additionally, the peak of the intensity was also more accurately captured by the M5LM-APRoe model. On the other hand, for the

M5LM-APRoe-SGS, the worse results than that of M5-APRoe is obtained in the turbulence region of x_1 > 4D. Two suggested reasons are provided here. One is that even with M5LM to reduce the Roe dissipation, the Smagorinsky model still provides too much SGS dissipation to the turbulence region of x_1 > 4D so the result is even worse than that of M5-APRoe. The other is that the classical Smagorinsky model is not so appropriate for the anisotropic turbulence such as the flow field in the thermal plume here. Based on the statistical result, it should be recognized that the Smagorinsky model couldn't improve the result in the present study.

The temporal power spectrum of the temperature fluctuation against the Strouhal number ($St = f \times D / U_0$) is obtained for two different locations (Fig. 4). One, denoted *P1*, is at the centre of the circular heat source but 0.6 m above the wall while the other, denoted *P2*, is at the edge of the circular heat source and also 0.6 m above the wall. Only the results of M5LM-APRoe and M5-APRoe are shown here to focus on the effect of the Roe dissipation term with the different reconstructions.

For *P1*, the results of M5LM-APRoe and M5-APRoe are similar. When the frequency is higher than the LES cut-off frequency, the −5/3 Kolmogorov power law is well captured. This is because the location of *P1* is in the fully turbulent region [10].

For the spectrum in *P2*, the result of ILES is similar to the distribution in *P1*. However, the M5LM-APRoe result presents a different distribution near the LES cut-off frequency. Moreover, the −5/3 Kolmogorov power-law decays more rapidly, following instead a −3 power decay law. This rapid decay is caused by the buoyancy force in the inertial-convective region, and it has been proposed as a result of numerical simulations [10,16] and experimental observations by Dai and co-workers [25]. As shown in Fig. 1(b), in P2, the over-dissipation in M5-APRoe enlarges the

turbulent structure. Hence, the fluctuations based on time in M5-APRoe will be overestimated owing to the production of the unphysically larger structure. The overestimated fluctuations cause the accumulation of energy at smaller scales. Meanwhile, the M5LM-APRoe can provide appropriate dissipation to correctly transfer energy from large to small scales. The result demonstrates that the M5LM-APRoe model captures the turbulence energy transfer induced by the buoyancy force.

6. Conclusion

A new compressible solver using implicit LES for laminar–turbulent transition in natural convection was developed. In this solver, M5LM is applied on APRoe referred to as M5LM-APRoe to improve the dissipation from the Roe dissipation term to be an implicit turbulence model. Besides, the Smagorinsky model with M5LM-APRoe named M5LM-APRoe-SGS is also performed to evaluate the effect of the SGS model. Comparisons of statistical quantities with DNS results show that most accurate results can be obtained with M5LM-APRoe. Moreover, the spectrum distribution of the temperature fluctuations shows that the M5LM-APRoe is also reliable in predicting the energy transfer driven by buoyancy forces in turbulence. Therefore, the current solver can be applied for the laminar–turbulent transition in natural convection with high temperature differences.

7. Acknowledgements

This work was supported by JSPS KAKENHI Grant Number JP19K14890.

References

[1] D.D. Gray, A. Giorgini, The validity of the Boussinesq approximation for liquids and gases, Int. J. Heat Mass Transf. 19 (1976) 545–551. doi:doi.org/10.1016/0017-9310(76)90168-X.

[2] J.M. Weiss, W.A. Smith, Preconditioning applied to variable and constant density flows, AIAA J. 33 (1995) 2050–2057. doi:10.2514/3.12946.

[3] P.L. Roe, Approximate Riemann solvers, parameter vectors, and difference schemes, J. Comput. Phys. 43 (1981) 357–372. doi:10.1016/0021-9991(81)90128-5.

[4] H. Paillere, C. Viozat, a. Kumbaro, I. Toumi, Comparison of low Mach number models for natural convection problems, Heat Mass Transf. 36 (2000) 567–573. doi:10.1007/s002310000116.

[5] E.L.I. Turkel, Preconditioned Methods for Solving the Incompressi and Low Speed Compressible Equations, J. Comput. Phys. 298 (1987) 277–298. doi:10.1016/0021-9991(87)90084-2.

[6] C.G. Li, M. Tsubokura, W.S. Fu, N. Jansson, W.H. Wang, Compressible direct numerical simulation with a hybrid boundary condition of transitional phenomena in natural convection, Int. J. Heat Mass Transf. 90 (2015) 654–664. doi:10.1016/j.ijheatmasstransfer.2015.06.058.

[7] G.E. Lau, G.H. Yeoh, V. Timchenko, J. a. Reizes, Large-Eddy Simulation of Turbulent Natural Convection in Vertical Parallel-Plate Channels, Numer. Heat Transf. Part B Fundam. 59 (2011) 259–287. doi:10.1080/10407790.2011.560815.

[8] G.E. Lau, G.H. Yeoh, V. Timchenko, J.A. Reizes, Large-eddy simulation of natural convection in an asymmetrically-heated vertical parallel-plate channel: Assessment of subgrid-scale models, Comput. Fluids. 59 (2012) 101–116. doi:10.1016/j.compfluid.2012.01.006.

[9] A.W. Vreman, An eddy-viscosity subgrid-scale model for turbulent shear flow: Algebraic theory and applications, Phys. Fluids. 16 (2004) 3670–3681. doi:10.1063/1.1785131.

[10] M. V. Pham, F. Plourde, K.S. Doan, Direct and large-eddy simulations of a pure thermal plume, Phys. Fluids. 19 (2007) 1–13. doi:10.1063/1.2813043.

[11] C. Meneveau, T.S. Lund, W.H. Cabot, A Lagrangian dynamic subgrid-scale model of turbulence, J. Fluid Mech. 319 (1996) 353–385.

doi:10.1017/S0022112096007379.

[12] E. Bou-Zeid, C. Meneveau, M. Parlange, A scale-dependent Lagrangian dynamic model for large eddy simulation of complex turbulent flows, Phys. Fluids. 17 (2005) 1–18. doi:10.1063/1.1839152.

[13] K. Loh, J.A. Domaradzki, The subgrid-scale estimation model on nonuniform grids The subgrid-scale estimation model on nonuniform grids, Phys. Fluids. 11 (1999) 3786–3792. doi:10.1063/1.870239.

[14] X.S. Li, C.W. Gu, Mechanism of Roe-type schemes for all-speed flows and its application, Comput. Fluids. 86 (2013) 56–70. doi:10.1016/j.compfluid.2013.07.004.

[15] B. Thornber, A. Mosedale, D. Drikakis, D. Youngs, R.J.R. Williams, An improved reconstruction method for compressible flows with low Mach number features, J. Comput. Phys. 227 (2008) 4873–4894. doi:10.1016/j.jcp.2008.01.036.

[16] F. Plourde, M.V. Pham, S.D. Kim, S. Balachandar, Direct numerical simulations of a rapidly expanding thermal plume: structure and entrainment interaction, J. Fluid Mech. 604 (2008) 99–123. doi:10.1017/S0022112008001006.

[17] W.S. Fu, W.H. Wang, C.G. Li, An investigation of natural convection in parallel square plates with a heated top surface by a hybrid boundary condition, Int. J. Therm. Sci. 84 (2014) 48–61. doi:10.1016/j.ijthermalsci.2014.04.009.

[18] K.H. Kim, C. Kim, Accurate , efficient and monotonic numerical methods for multi-dimensional compressible flows Part II : Multi-dimensional limiting process, 208 (2005) 570–615. doi:10.1016/j.jcp.2005.02.022.

[19] D. Talukdar, C.G. Li, M. Tsubokura, Numerical investigation of buoyancy-driven compressible laminar flow using new method preconditioned all-speed roe scheme, Int. Commun. Heat Mass Transf. 98 (2018) 74–84. doi:10.1016/j.icheatmasstransfer.2018.08.007.

[20] W.-S. Fu, C.-G. Li, M. Tsubokura, Y. Huang, J.A. Domaradzki, An Investigation of Compressible Turbulent Forced Convection by an Implicit Turbulence Model for Large Eddy Simulation, Numer. Heat Transf. Part A Appl. 64 (2013) 858–878. doi:10.1080/10407782.2013.807663.

[21] C. Li, M. Tsubokura, An implicit turbulence model for low-Mach Roe scheme using truncated Navier–Stokes equations, J. Comput. Phys. 345 (2017) 462–474. doi:10.1016/j.jcp.2017.05.032.

[22] Y. Cheng, V.M. Canuto, Determination of the Smagorinsky – Lilly constant, Phys. Fluids. 9 (1998). https://web.stanford.edu/group/ctr/ResBriefs97/oberlack.pdf.

[23] T.T. Bui, A parallel , Finite-volume algorithm for large-eddy simulation of turbulent flows, Comput. Fluids. 29 (2000) 877–915. doi:10.1016/S0045-7930(99)00040-7.

[24] W.-S. Fu, C.-G. Li, W.-F. Lin, Y.-H. Chen, Roe scheme with preconditioning method for large eddy simulation of compressible turbulent channel flow, Int. J. Numer. Methods Fluids. 61 (2009) 888–910. doi:10.1002/fld.1987.

[25] Z. Dai, L.K. Tseng, G.M. Faeth, Velocity statistics of round, fully developed, buoyant turbulent plumes, J. Heat Transfer. 117 (1995) 138–145. doi:10.1115/1.2822294.

Table Captions

Table I Computation parameter settings

Table 1. Computation parameter settings

Time step Δt	2×10^{-3} s
Temperature of heat surface T_h	673 K
Diameter of heat surface D	0.1 m
Characteristic buoyancy velocity	$U_0 = \sqrt{gD\Delta T / T_0}$ =1.11 m/s
Domain size ($l_1 \times l_2 \times l_3$)	$1.024\times0.512\times0.512$ m^3
$\Delta x_1 \times \Delta x_2 \times \Delta x_3$	$0.004\times0.004\times0.004$ m^3
$N_1 \times N_2 \times N_3$	$256\times128\times128$
$N_1 \times N_2 \times N_3$ in DNS [10]	$1200\times720\times720$

Figure Captions

Fig. 1 Physical model and vorticity isosurface

Fig. 2 Comparison of normalized values

Fig. 3 Comparison of turbulence intensities

Fig. 4 Temporal power spectra of temperature fluctuations

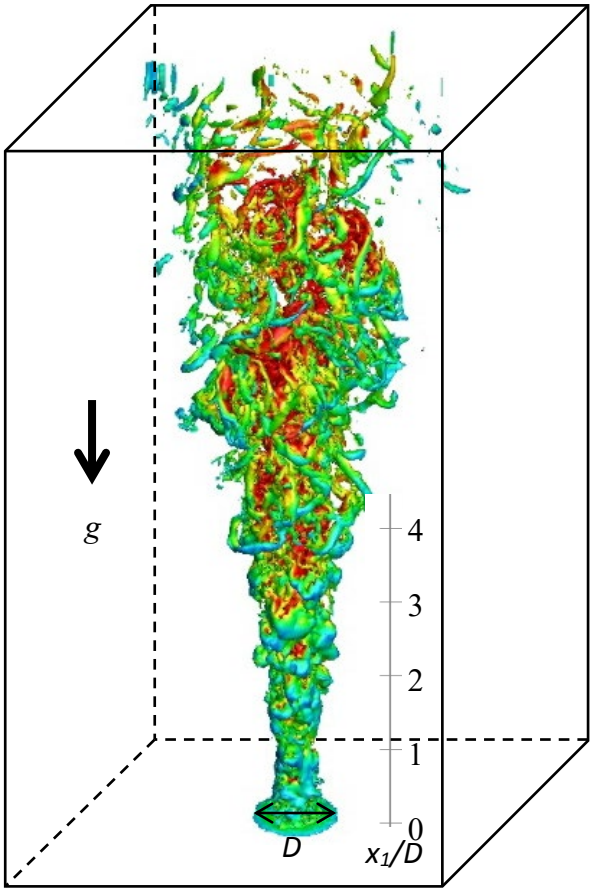

(a) Physical model

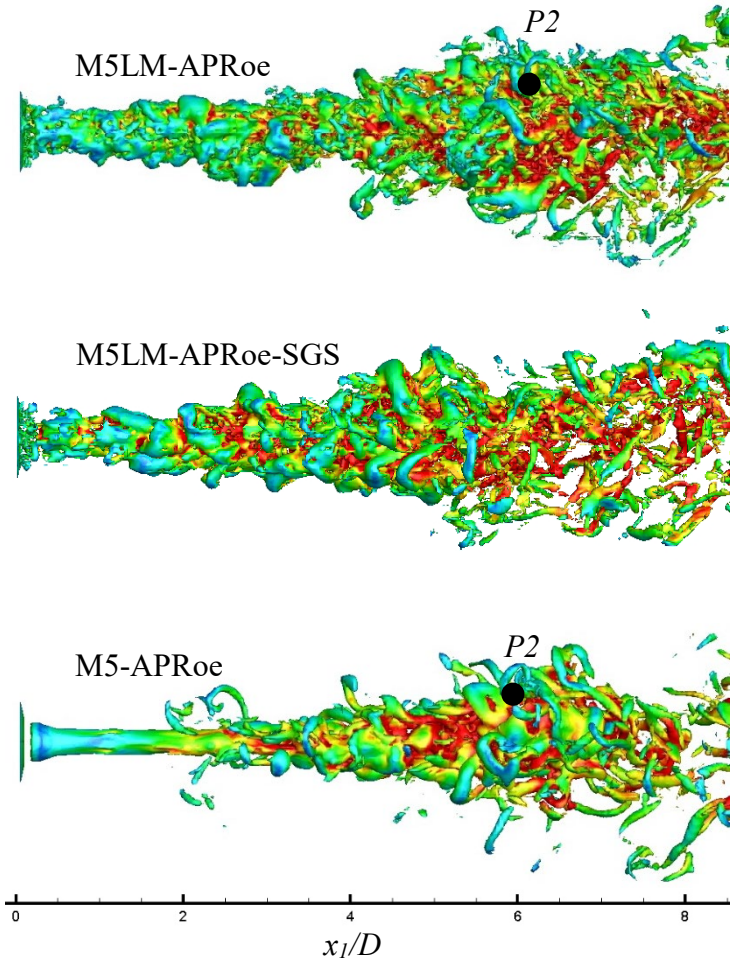

(b) Comparison of the vorticity isosurface

Fig. 1. Physical model and the vorticity iso-surface

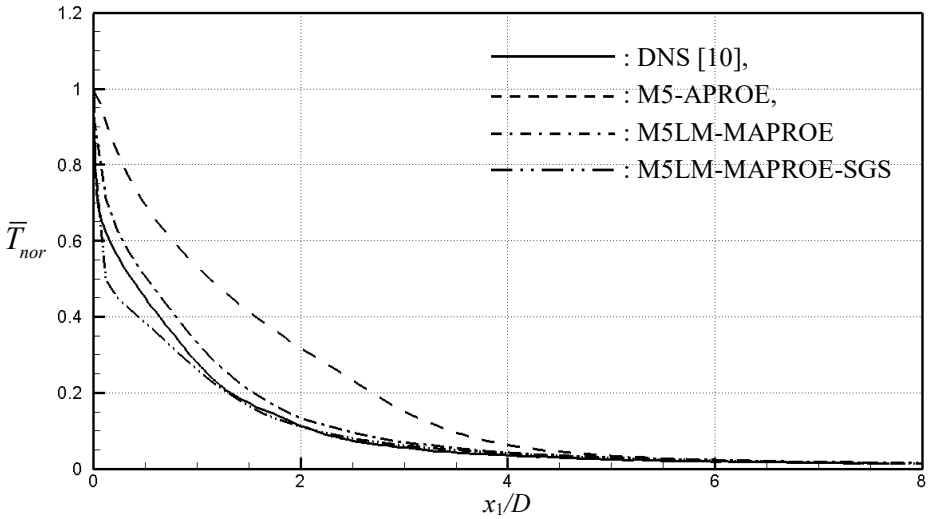

(a) Mean temperature

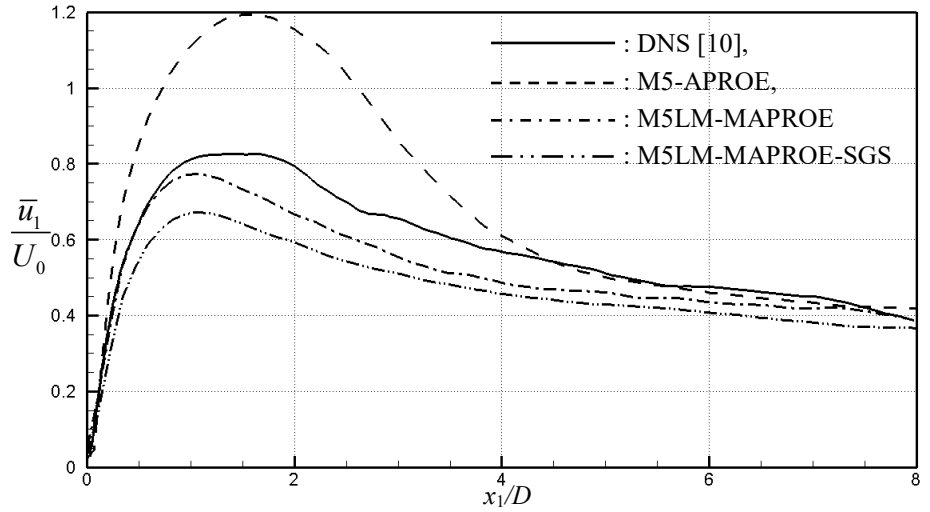

(b) Mean velocity

Fig. 2. Comparison of normalized values

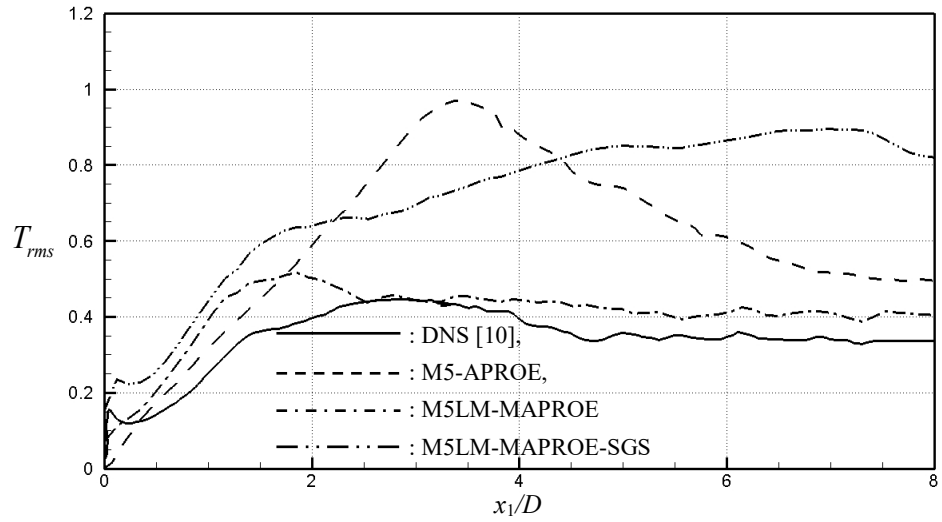

(a) Temperature

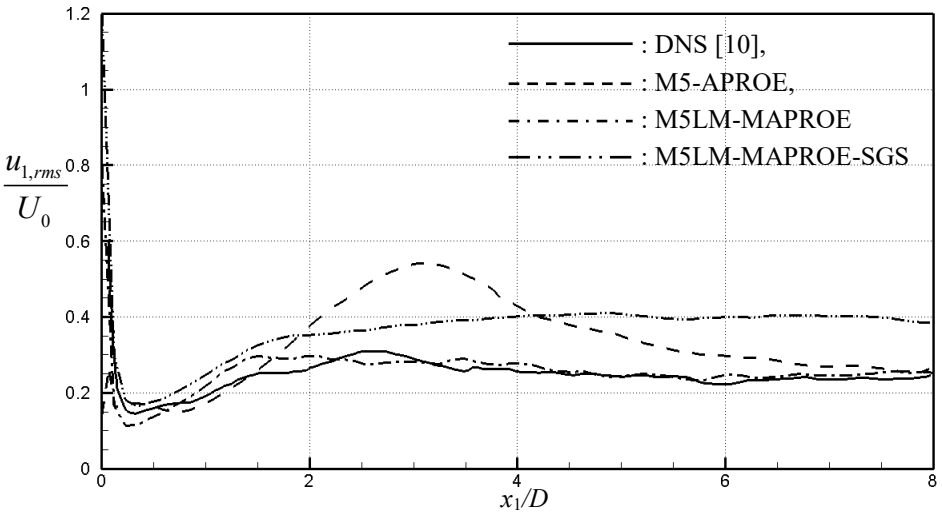

(b) Velocity

Fig. 3. Comparison of turbulence intensities

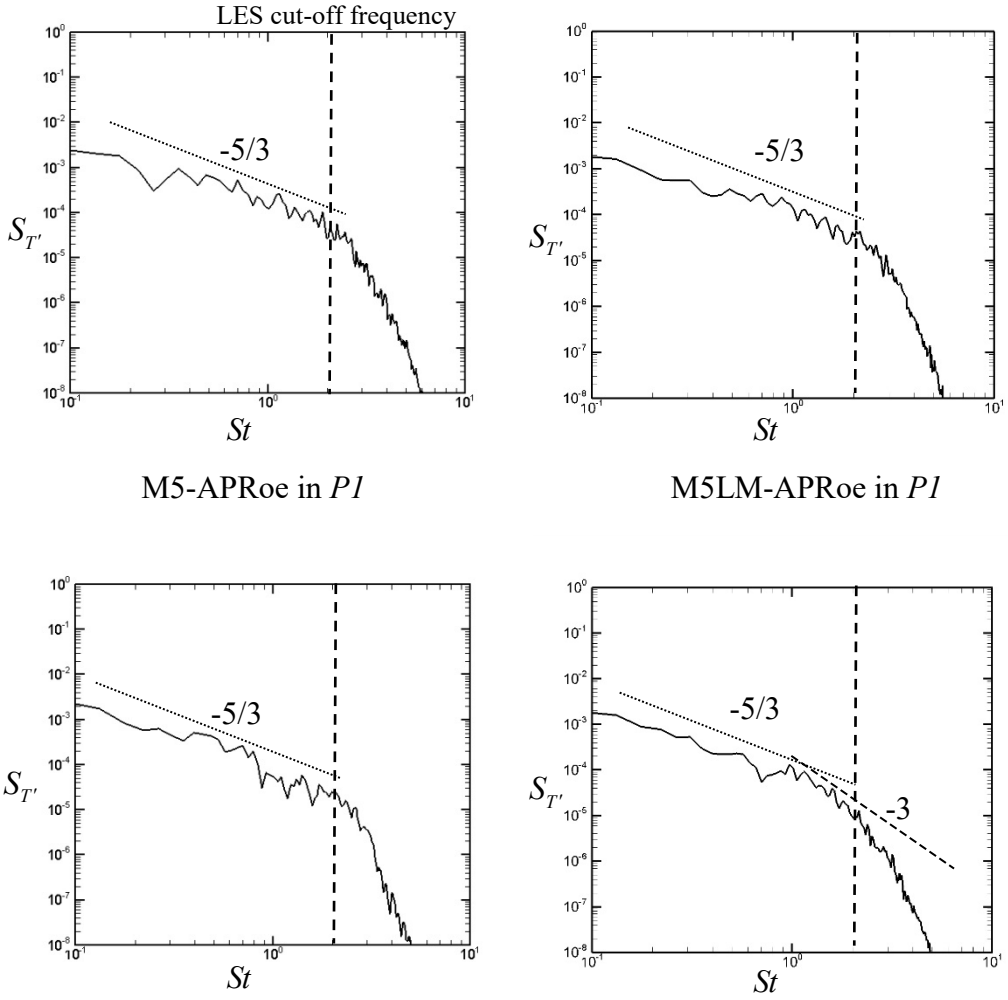

Fig. 4. Temporal power spectra of temperature fluctuations